Colloids and Surfaces B: Biointerfaces 132 (2015) 27–33

Contents lists available at ScienceDirect

Colloids and Surfaces B: Biointerfaces

journal homepage: www.elsevier.com/locate/colsurfb

Black hemostatic sponge based on facile prepared cross-linked graphene

Kecheng Quan[a,1], Guofeng Li[a,1], Di Luan[a], Qipeng Yuan[a], Lei Tao[b], Xing Wang[a,*]

[a] The State Key Laboratory of Chemical Resource Engineering, Beijing University of Chemical Technology, Beijing 100029, PR China
[b] The Key Laboratory of Bioorganic Phosphorus Chemistry & Chemical Biology (Ministry of Education), Department of Chemistry, Tsinghua University, Beijing 100084, PR China

ARTICLE INFO

Article history:
Received 10 February 2015
Received in revised form 29 April 2015
Accepted 30 April 2015
Available online 11 May 2015

Keywords:
Graphene
CGS
Hemostatic sponge
Hemostasis
Clotting

ABSTRACT

In this study, we demonstrate for the first time the remarkable hemostatic performance of a cross-linked graphene sponge (CGS) as a superb hemostat. The CGS can absorb plasma immediately (<40 ms) to form a blood cell layer and promotes subsequent clotting. The interaction between the interface of the CGS and blood cells reveals that the fast blood coagulation is primarily attributed to the enrichment of hemocytes and platelets on the wound surface. An *in vitro* dynamic whole-blood clotting test further highlights the effectiveness of the CGS. Considering the facile preparation, low cost, nontoxicity, and long shelf life of the portable black sponge, the CGS has great potential for trauma treatment.

1. Introduction

Graphene, a two-dimensional (2D) monolayer of carbon atoms, has been studied in recent years as one of the most useful nanomaterials [1–5]. Recently, applications of graphene-based materials in biomedical and pharmaceutical fields have attracted much attention due to the materials' biocompatibility, good water dispersity, potential for functional modification, and unique optical and electronic properties. As reported, graphene-based materials have been widely utilized as platforms for drug delivery [6,7], biosensors [8–10], cellular imaging [11–13], and cancer therapy [14–16], demonstrating their promising prospects for use in biomaterials. Furthermore, for safe applications *in vivo*, significant efforts have been undertaken to improve the biocompatibility of graphene-based materials including amine modification and heteroatom doping [6,8,17,18]. However, graphene and its derivatives are xenobiotic substances. Thus, utilizing their superb characteristics in *in vitro* biomedical applications should be actively explored and developed. To the best of our knowledge, there are few studies that have focused on graphene-based materials for use in the field of hemostasis, although hemostatic materials are vital in both civilian and military medicine because rapid hemostasis is essential for optimal recovery and even survival [19,20]. Traditional hemostatic agents, such as zeolite [20,21] and mesoporous silica [22–24], mainly depend on their quick plasma absorbability to accelerate the aggregation of blood cells, while chitosan-based hemostatic materials [25,26] promote blood coagulation by charge effect – positively charged chitosan attracts negatively charged red blood cells to form a layer of blood clot. These studies especially on the hemostatic mechanisms have a great significance for the development of new generation of hemostatic materials.

Among graphene-based materials, cross-linked graphene, generally prepared from a suspension of graphene oxide (GO) nanosheets with suitable chemical linkers, has exhibited prominent advantages, including large pore volumes, high surface areas, low density, and ideal structural stability [27–31], which make it suitable for hemostatic applications. Cross-linked graphene possesses a remarkable capability for rapid liquid absorption [32,33], which inspired us to develop a novel black hemostatic sponge based on its three-dimensional (3D) structure for rapidly absorbing plasma and thus increasing the concentration of blood cells to accelerate blood clotting [21,34]. In this study, we demonstrate for the first time a cross-linked graphene sponge (CGS) as an exemplary hemostat and its outstanding hemostatic performance.

* Corresponding author. Tel.: +86 1064447747; fax: +86 1064416428.
E-mail address: wangxing@mail.buct.edu.cn (X. Wang).
[1] These authors contributed equally to this work.

http://dx.doi.org/10.1016/j.colsurfb.2015.04.067
0927-7765/

2. Experiments

2.1. Preparation and characterization of the CGS

A 200 μl volume of ethylenediamine (EDA) used as a cross-linking agent was added to 20 ml GO dispersion (3 mg ml^{-1}, prepared *via* a modified Hummers' method [35]). The mixture was sealed in a hydrothermal synthesis reaction kettle (inside diameter, 4 cm) and heated to 96 °C for 6 h to obtain a GO hydrogel. After freeze-drying for 48 h, the GO aerogel (GOA) was embathed with ethyl alcohol in a Soxhlet extractor for 48 h to remove the unreacted EDA. Next, the purified GOA was dried at ambient temperature for 24 h, and under air conditions, it was treated with microwave radiation (800 W) for 5 s to obtain the CGS (3 cm diameter, 1.2 cm thickness).

Scanning electron microscopy (SEM) was performed using an S-4700 Hitachi microscope. The cross sections of the CGS and GOA samples were observed at different resolutions to compare the internal structure before and after microwave treatment. Brunauer–Emmet–Teller (BET) surface area measurements were determined by the nitrogen gas adsorption method by using a Micromeritics ASAP 2020 analyzer at liquid nitrogen temperature. Methylene blue (MB) dye adsorption test was further performed to evaluate the surface area according to the reported method [36]. An elemental analyzer Vario ELcube was used to conduct elemental analysis. The CGS and GOA samples were processed into powder, and the contents of C, H, O, and N were determined.

2.2. Evaluation of the hemostatic performance

A droplet of blood was dropped onto the CGS surface, and a high-speed camera (40 ms per frame) was used to record the entire process of blood absorption. The rate of blood absorption was calculated based on the frame rate and alignment. Next, the CGS was dipped in a blood pool to absorb blood adequately. The CGS was weighed twice before and after dipping to determine the weight of absorbed blood. The blood absorption capability of the CGS was presented as the mass ratio of blood and CGS. As a control, the water absorption rate and capability were tested using the same method mentioned above.

A rat-tail cutting experiment was used to evaluate the hemostatic performance of the CGS. Healthy male Sprague-Dawley (SD) rats (250 ± 20 g, 7 weeks of age) were used as animal models. They were purchased from the Vital (Charles) River Laboratory, Beijing, China. Animals were treated and cared for in accordance with the National Research Council's Guide for the care and use of laboratory animals. Each rat was raised in a single cage. The rats were raised for 3 days in a standard environment to ensure a healthy physiological state. All rats were anesthetized with 1.25 ml 10% chloral hydrate (0.5 ml per 100 g) before surgery. Each rat tail, measuring 16 cm in length, was cut at 6 cm from the tip by surgical scissors. The wound section was covered with the CGS directly to control bleeding with slight pressing. The hemostatic time was recorded. The CGS was weighed before and after hemostasis to determine the weight of the blood loss. Gauze sponge served as a control in this study.

2.3. Interaction between the interface of CGS and blood cells

2.3.1. Morphology study of blood cells

A total of 1 ml volume of phosphate buffered saline (PBS; pH 7.4) with 50 μl ACD-whole blood was added onto the CGS (3 cm diameter, 1.2 cm thickness) surface. The material containing whole blood was incubated for 3 min at 37 °C. The sample was then gently rinsed three times with PBS and immobilized with 2.5% glutaraldehyde for 2 h at 4 °C. Blood cells were dehydrated with 50, 60, 70, 80, 90 and 100% ethanol for 10 min. The samples were freeze-dried for 12 h prior to SEM observation [25].

2.3.2. Blood cell adhesion

A small piece of the CGS (1 × 1 cm^2, 0.25 cm thickness) was immersed in 10 ml PBS for 2 h at 37 °C. Next, 0.5 ml ACD-whole blood was added. The material containing whole blood was incubated for 1 h at 37 °C. The sample was then treated according to the above-mentioned method prior to SEM observation.

2.3.3. Platelet adhesion

The ACD-whole blood was centrifuged at 300 × *g* for 20 min at 4 °C to obtain platelet-rich plasma (PRP). A portion of the PRP was further centrifuged at 2000 × *g* for 20 min at 4 °C to obtain platelet-poor plasma (PPP). The platelet concentration was adjusted to 1×10^5 platelets μl^{-1} by adding PPP to PRP, and the number of platelets was counted by a hemocytometer. The CGS (1 × 1 cm^2, 0.25 cm thickness) was then placed on a Petri dish covered with PRP and incubated for 1 h at 37 °C. The sample was treated according to the above-mentioned method prior to SEM observation [22,37].

2.4. In Vitro *dynamic whole-blood clotting*

Total 50 μl volume of fresh blood drawn from SD rats was directly dropped onto four test groups, including a blank, Ca^{2+} (4 μl $CaCl_2$ solution, 0.2 mol L^{-1}), gauze sponge, and the CGS in 50 ml glass beakers, respectively. The volume of the gauze sponge was same as that of the CGS (1 × 1 × 0.25 cm^3). Each group was allowed to interact for 30, 60, 120, 180, and 240 s. Then, 10 ml distilled water was added slowly down the inside wall of the beaker without disturbing the clotted blood. The beaker was shaken slightly to dissolve free RBCs. The absorbance of each of the resulting samples was measured by an ultraviolet spectrophotometer at 542 nm. As a reference value, the absorbance of 50 μl fresh blood in 10 ml distilled water was measured. The content of hemoglobin was quantified by the following equation: Hemoglobin absorbance = $I_s/I_r \times 100\%$, where I_s is the absorbance of the resulting sample, and I_r is the absorbance of the reference value. This experiment was repeated three times with different healthy SD rats under the same conditions [38,39].

2.5. Cytotoxicity evaluation

L929 mouse fibroblast cells (purchased from Cell Resource Center, IBMS, CAMS/PUMC, Beijing, China) were adjusted to 8×10^5 cells ml^{-1} in complete medium (CM), which consisted of 90% RPMI-1640 medium, 10% fetal bovine serum (FBS), and 1% antibiotics (100 units ml^{-1} penicillin and 100 units ml^{-1} streptomycin). The cell suspension was added into 96-well plates (100 μl per well) and incubated for 24 h at 37 °C in an air environment of 5% CO_2. Meanwhile, 5 ml RPMI-1640 medium was added to the CGS as the test group, and an equal volume of RPMI-1640 medium was added to an empty bottle as the negative control group. After 24 h, the impregnating solution was removed from the test group and added to the corresponding CM. After 48 h of incubation, cell viability was determined by a MTT assay kit based on the manufacturer's instructions. The relative growth rate (RGR) of the cells was calculated according to the following formula: RGR = $Abs_{490\ test}/Abs_{490\ control} \times 100\%$. Finally, the toxicity grade was assessed based on the RGR. This experiment was repeated three times [40,41].

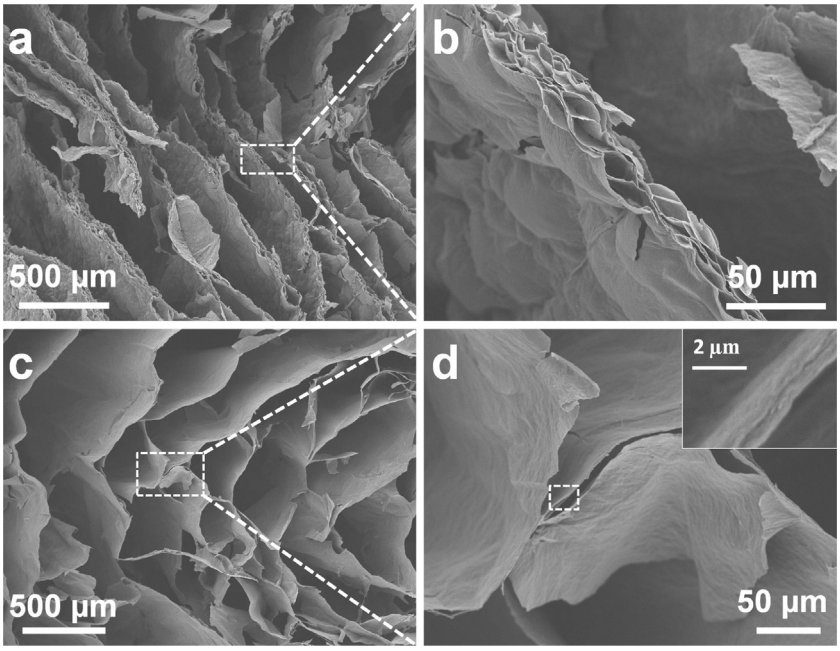

Fig. 1. (a) SEM image of the hierarchical porous structures of CGS. (b) The enlarged porous structure of the CGS cell wall. (c) SEM image of the cross profile of GOA. (d) The enlarged GOA cell wall. The inset shows a stacked lamellar structure of GO nanosheets.

3. Results and discussion

3.1. Preparation and characterization of the CGS

The CGS was obtained *via* an optimized version of Hu's method [32] as described above. To improve the potential hemostatic properties and practical applications, we optimized the production process by making two changes. First, microwave irradiation was conducted in air, which not only simplified the manufacturing process but also increased the cavity structure of the sponge to enhance the liquid absorption rate by a large margin. Second, the dosage of the EDA linker was optimized to v/v = 1:100 when mixed with the GO solution, which ensured that a suitable sponge material could be created.

The internal structure of the CGS is presented in Fig. 1a. The CGS exhibited a hierarchical porous structure with a large number of small cavities measuring from tens to hundreds of micrometers along the cell wall (Fig. 1b), unlike those observed for the GOA (Fig. 1c). This network maintained a strong interconnection between the building layers to prevent the intense microwave treatment from breaking down the monolithic structure. After only 5 s of microwave treatment, most of the assembled graphene

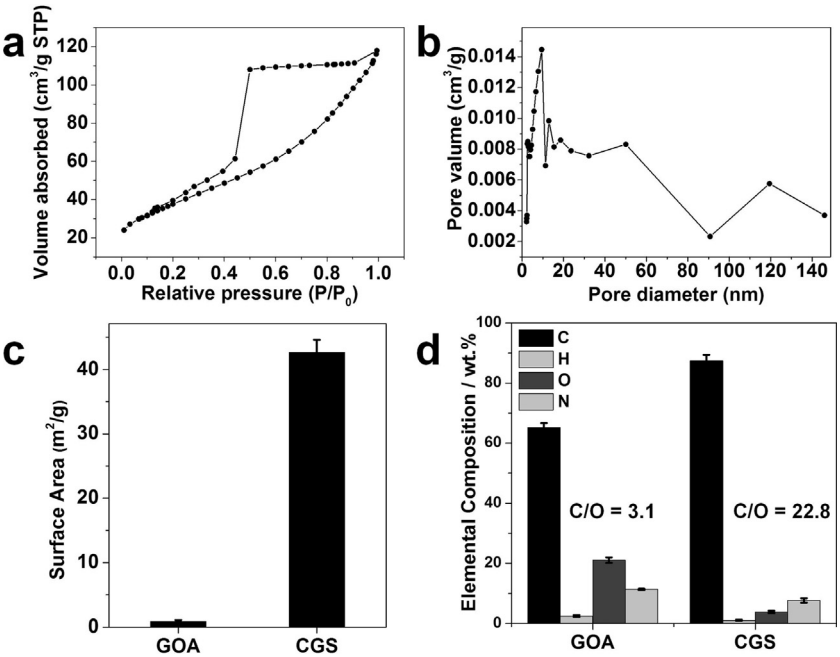

Fig. 2. (a) The N_2 adsorption–desorption isotherm of the CGS. (b) The BJH pore size distribution. (c) BET surface area of CGS and GOA. (d) Elemental analysis of CGS and GOA. Data values corresponded to mean ± SD ($n = 3$).

sheets that made up the cell walls separated from each other and formed a cellular structure in the CGS (Fig. 1b). On the other hand, all of the graphene sheets were stacked closely in the GOA cell wall (Fig. 1d). This prominent difference suggests that the strong energy of the microwaves interrupted the interaction between the graphene sheets and observably increased the specific surface area of the CGS.

Fig. 2a shows the N_2 adsorption–desorption isotherm of the CGS. According to the IUPAC classification, the curve is characterized by type-IV with a H2 hysteresis loop at a relative pressure P/P_0 ranging from 0.4 to 1.0 [42]. It indicates that irregular size and shape of pores exists in the CGS material. As a result, a multi-peak curve was found in the analysis of BJH pore size distribution (Fig. 2b). The BJH adsorption average pore diameter (4 V/A) is 5.7 nm. Based on the data of relative pressure P/P_0 ranging from 0.5 to 3.5, the calculated BET surface area of the CGS ($42.9 \pm 1.9\ m^2\ g^{-1}$) was significantly greater than that of the GOA ($0.8 \pm 0.2\ m^2\ g^{-1}$), as shown in Fig. 2c. These data indicate that after being cross-linked by EDA, a large number of the GO sheets aggregated into stacks, which greatly decreased the surface area of the GOA compared with the theoretical surface area of single-layer graphene sheets [23,43,44]. However, after the microwave puffing procedure, this simple and strong reduction process largely increased the surface area of the CGS by a factor of approximately 54.

In addition, dye adsorption test was also performed to evaluate the specific surface area [36]. It was determined in an ethanol suspension with MB dye as a probe. As a result, the specific surface area of the CGS ($854.9 \pm 30.3\ m^2\ g^{-1}$) was also greater than that of the GOA ($459.3 \pm 43.6\ m^2\ g^{-1}$). Compared with the BET method, the absolute values were enlarged. It might be owing to the different molecular interactions. Furthermore, the increment became less. We speculated that MB molecules were absorbed in the GOA and in the CGS with different way, because the GOA has much more carboxyl and hydroxyl groups (ionic and hydrogen bonding interactions) than the CGS (π–π interaction). After microwave puffing, most of the carboxyl and hydroxyl of the GOA were removed, which reduced the adsorption of MB molecules in the CGS to a large extent.

Elemental analysis (Fig. 2d) showed that the C/O mass ratio increased to 22.8 (CGS, C 87.44; O 3.83) from 3.1 (GOA, C 65.17; O 21.05), indicating that during the high-energy treatment, most of the surface and internal oxygenic functional groups had been removed. Most of the EDA linkers survived the reduction, as the content (%) of N element was 7.66 for the CGS compared with the initial value of 11.32 for the GOA, thus supporting the structural stability of the final CGS product. In addition, according to the experiments, using less linker (v/v < 1:250) [32] did not produce adequate microwave irradiation under air conditions. This material was too loose to maintain the shape of the sponge after applying slight pressure, which limited its practical application. More linker (v/v > 1:50) made the sponge too tight to exhibit sufficient absorbability, although microwave puffing could create a porous structure. These results are not presented here.

3.2. Evaluation of the absorption ability

High-speed imaging showed that a droplet of blood could be absorbed onto the CGS within 40 ms, as shown in Fig. 3b and 3c, illustrating an ultrafast blood absorption rate. Furthermore, the CGS could absorb as much as 147 times its own weight of blood. As a control, the same phenomena were observed for water; the CGS could absorb a droplet within 40 ms and approximately 112 times its own weight of water (Fig. 3a). The time required for the GOA to absorb as much liquid (water and blood) was more than 200 ms (Fig. 3a), which demonstrated that microwave puffing could significantly enhance absorption. Therefore, the ultrafast absorption of the CGS provides a theoretical foundation for rapid hemostasis.

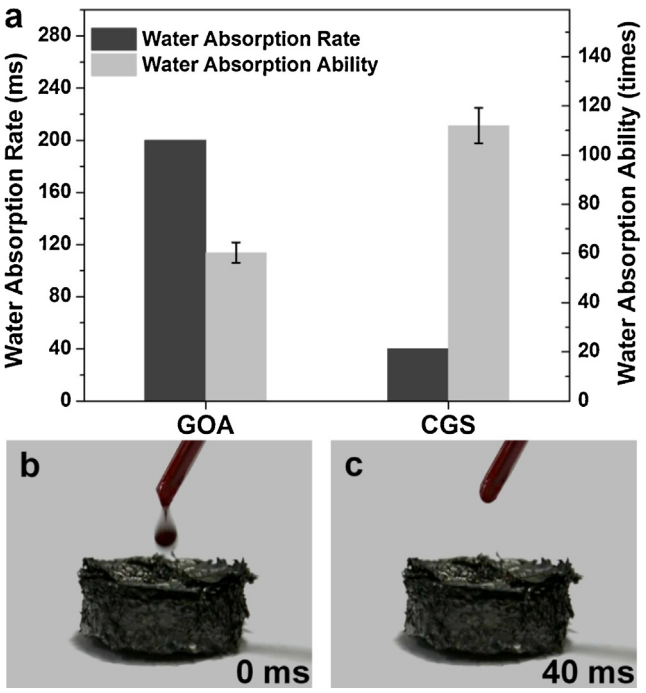

Fig. 3. (a) Water absorption rate and capability of CGS and GOA. Data values corresponded to mean ± SD ($n = 6$). (b) and (c) Photographs of the blood absorption process on the CGS sample.

Specifically, once blood contacts the CGS, the moisture of the blood is absorbed immediately, forming a layer of blood cells between the wound and the CGS surface. This cell layer clots instantly to achieve rapid hemostasis.

3.3. Evaluation of hemostatic performance

Fig. 4a shows a representative result obtained from the rat-tail cutting experiments using the black CGS hemostat (gauze sponge was used as a control). The bleeding stopped rapidly, and the wound clotted with only a small number of graphene sheets. The bleeding time and blood loss are recorded in Fig. 4b. Among the six parallel experiments, the mean bleeding time was 201 ± 46 s, and the mean blood loss was 0.085 ± 0.025 g. Ruling out the individual differences, the CGS could control bleeding within 240 s, whereas the gauze control could only stop bleeding but did not promote coagulation even after 10 min [45]. The value of gauze sponge is therefore not represented in Fig. 4b. These results demonstrated that the CGS could play an excellent role in hemostasis just by being in contact with the wound.

3.4. Interaction between the interface of CGS and blood cells

To further reveal the hemostatic mechanism, scanning electron microscopy (SEM) was employed to observe the surface adhesion and morphologies of blood cells and platelets [22,25,37] on the CGS. Firstly, the cell morphology for the fast absorption of whole blood was studied by dropping blood onto the CGS surface. The mass of blood was far lower than the capacity limit of the CGS absorption to simulate the actual hemostatic process *in vitro*. Fig. 5a shows the SEM image of blood cells adsorbed on the CGS surface. A large amount of red blood cells (RBCs) gathered on the material surface, and some of them stretched out spiny pseudopodia, as shown in the enlarged image Fig. 5a′ (marked by the white arrows), where partial gathered RBCs also altered their shape from distinctive biconcave disks to irregular deformations. The above phenomena illustrated that a clotting layer formed on the CGS surface and blood cells

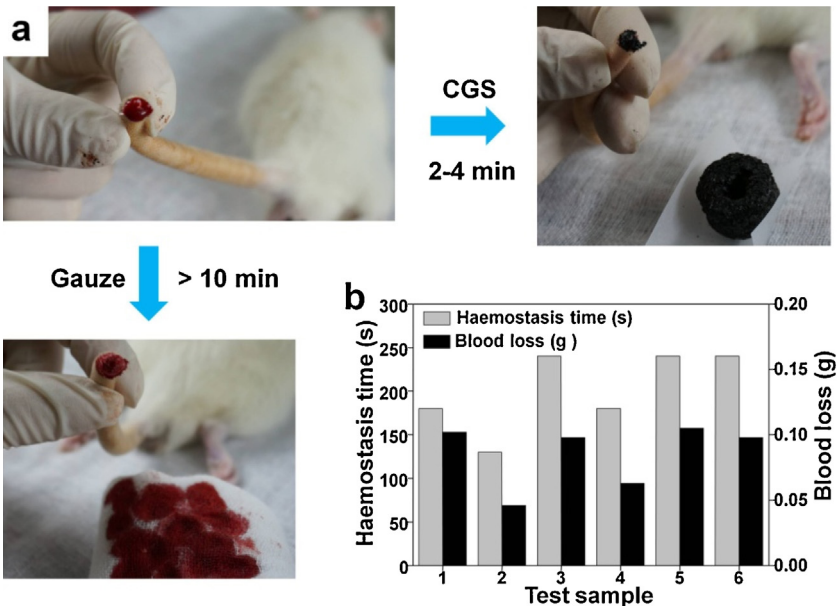

Fig. 4. Evaluation on the hemostatic performance of CGS. (a) The hemostatic effect of the CGS and the control group of gauze sponge, just by contacting with the wound. (b) The hemostasis time and blood loss of six CGS samples. The mean ± SD bleeding time is 201 ± 46 s and blood loss is 0.085 ± 0.025 g (n = 6).

produced physiological changes in this layer. Therefore, rapidly increasing concentration of blood cells could promote their aggregation and deformation on the CGS surface to accelerate blood coagulation.

However, in the above experiment, we were not sure whether the CGS could affect the blood cell physiological action during the whole coagulation process. To study the effect at the interface, a selective adhesion test of blood cells was conducted by

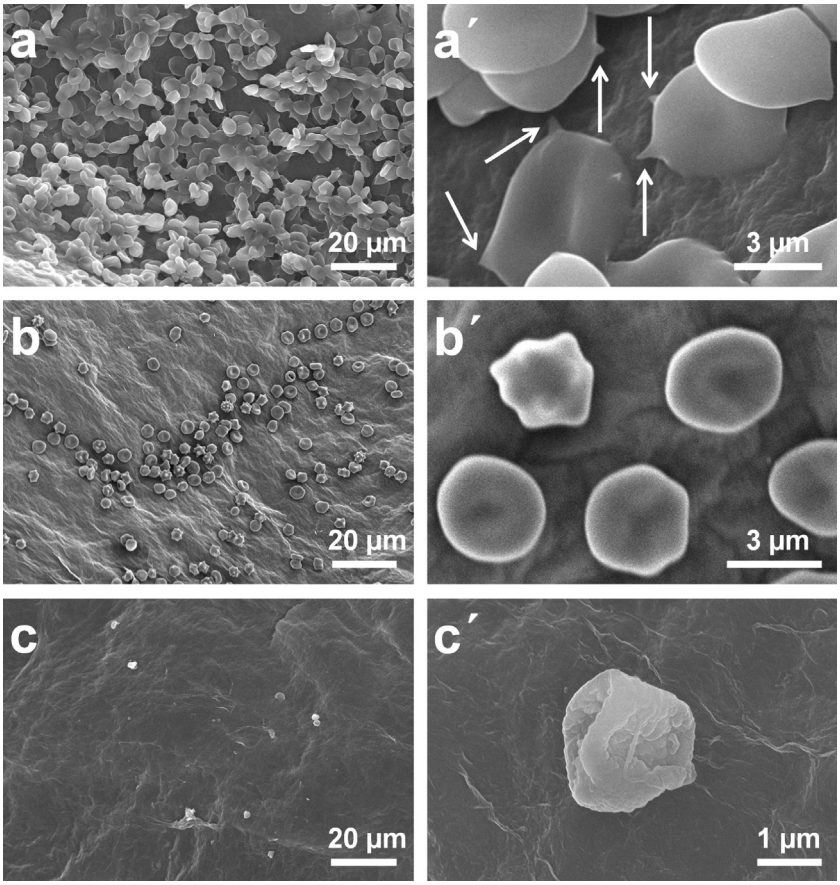

Fig. 5. SEM images of blood cells and platelets adhesion on the CGS surface. (a) Morphology of whole blood fast absorption. (a′) RBCs generated spiny pseudopodia. (b) Selective adsorption of blood cells. (b′) Blood cells with regular shape. (c) A few platelets adhered on the CGS. (c′) A magnified image of a resting platelet shown in (c).

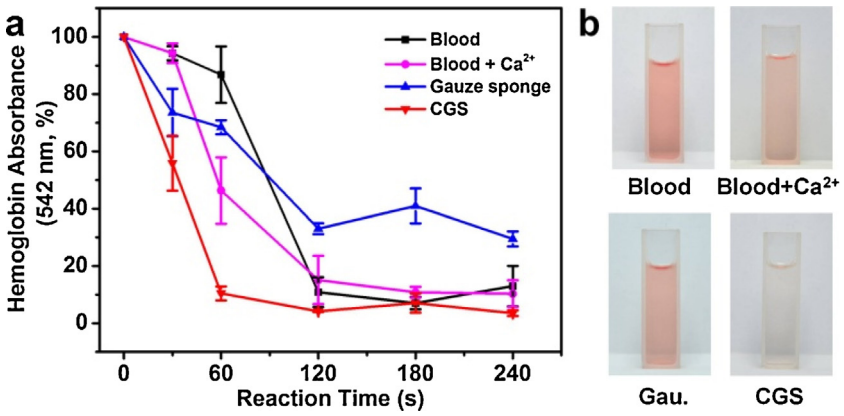

Fig. 6. (a) *In vitro* dynamic whole-blood clotting evaluation of CGS and control; Data values corresponded to mean ± SD ($n = 6$). (b) Photographs of the corresponding aqueous solutions of hemoglobin after 60 s.

immersing a piece of the CGS into a blood culture media and then adding a few drops of blood into the media to assay the interactions between cells and the material surface. As shown in Fig. 5b, a distinct amount of blood cells spread on the CGS surface, but none of them showed deformation or aggregation. Additionally, no spiny pseudopodia for RBC were found (Fig. 5b′). This phenomenon indicated that the CGS would not affect blood cells physiological action. In addition, in the above assay, almost no platelets were found in the SEM images. Therefore, platelet attachment on the CGS surface was further investigated through incubation with platelet-rich plasma (PRP). Fig. 5c and 5c′ shows the resulting SEM images. Only a few platelets adhered on the CGS surface (Fig. 5c), and the attached platelets displayed regular resting shape (Fig. 5c′). In other words, the CGS could not induce platelets aggregation or activation. These phenomena indicated that to a certain degree the CGS surface was hemocompatible. It was reported that N-doped or amine-modified graphene had good hemocompatibility [6,18]. In the CGS 3D structure, as mentioned above, EDA linkers introduced amine modification on the GO sheets and linkers rather than oxygenic groups that survived the microwave irradiation. As a result, through interacting with the graphene samples, platelets and RBCs would not be activated to change their morphologies.

Because the morphology test (Fig. 5a) vividly simulated the process of blood coagulation when the wound contacted with the CGS and the adhesion test (Fig. 5b and 5c) revealed the interfacial hemocompatibility of the fabricated material, the experiments demonstrated that the blood coagulation at the site of bleeding was mainly due to the concentration of native elements, such as hemocytes and platelets, *i.e.*, the fast adsorption process played a curial role in clot formation.

3.5. In Vitro *Dynamic whole-blood clotting*

Based on the understanding of the above-mentioned hemostatic mechanism of the CGS, a dynamic whole-blood clotting assay [38,39] was conducted to assess the blood clotting capability of the CGS *in vitro*. In this assay, fresh blood without anticoagulant was directly added to the CGS and gauze sponge (negative control). As control specimens, the same amount of blood was added to one beaker (blank control) and another beaker containing Ca^{2+} (a coagulation factor, positive control). The blood clotting capability was quantitatively determined using an ultraviolet spectrophotometer at 542 nm. The absorbance value represented the amount of hemoglobin in free RBCs. Four test samples interacted with fresh blood for different periods. As shown in Fig. 6a, over the initial 60 s, the absorbance value of the CGS was far lower than that of the other groups. For all control groups, fresh blood did not clot within 60 s, as indicated by the high absorbance value that was measured. The blood in the CGS clotted almost completely after 60 s, whereas the other control groups required 120, 180, and 240 s. We deduced that the CGS could accelerate blood clotting within the initial 60 s, when the blood coagulants naturally had not yet exerted their effects (Fig. 6b).

Another physiological reason derived from fast absorbing of plasma may also contribute to the quick clotting. Plasma inhibits blood clotting due to the existence of anticoagulant factors, which is why normal blood *in vivo* will not clot. Once outside of the body, these factors will lose activity quickly. Sixty seconds may be the natural threshold because the absorbance values of the control groups plummet after this time point. Because the CGS can rapidly absorb plasma, the anticoagulant factors are separated from whole blood, resulting in a quick clotting of blood cells by activating the inherent clotting system. This test clearly revealed that the CGS had the capability to perform blood clotting rapidly once blood made contact with it, perhaps independently of clotting factors, such as the Ca^{2+} used in this study.

3.6. *Cytotoxicity evaluation*

Because the CGS is a chemically modified biomaterial, its biocompatibility is a critical factor for practical applications, although, in our opinion, the main medical application will be the treatment of traumatic bleeding. The cytotoxicity of the CGS was evaluated by an MTT assay [40,41]. The relative growth rate (RGR) was 95.7 ± 7.0% for the CGS with respect to the growth rate of the culture dish control; thus, the CGS was proved to be noncytotoxic. According to the standard toxicity rating, the CGS was rated as grade 1, making it safe to use for traumatic bleeding.

4. Conclusions

We developed a novel trauma hemostatic material based on a CGS that could rapidly stop bleeding in approximately 2–4 min. The CGS absorbs plasma rapidly to increase the concentration of hemocytes and platelets on the wound surface, thus promoting blood coagulation. In-depth studies revealed that the hemostatic process on the CGS surface mainly depended on the physical absorption process instead of clotting factors. To the best of our knowledge, this is the first report on the use of a graphene material as a hemostatic agent. Compared with traditional hemostatics, such as zeolite [20,21], mesoporous silica [22–24], and chitosan hemostatic materials [25,26], the CGS has many advantages, including facile preparation, low cost, portability due to its ultra-light weight, long shelf life, and nontoxicity. Although the hemostatic effect can still

be improved, this black hemostatic sponge exhibits great potential in treating trauma bleeding.

Acknowledgments

The authors thank the National Natural Science Foundation of China (21204004), the Beijing Natural Science Foundation(2132040), the Specialized Research Fund for the Doctoral Program of Higher Education(20120010120011), the Open Project of State Key Laboratory of Chemical Resource Engineeringand the Fund amental Research Funds for Central Universities (YS1407) for funding support.

References

[1] A.K. Geim, K.S. Novoselov, Nat. Mater. 6 (2007) 183.
[2] X. Huang, X. Qi, F. Boey, H. Zhang, Chem. Soc. Rev. 41 (2012) 666.
[3] Z. Xu, C. Gao, Nat. Commun. 2 (2011) 571.
[4] X. Cao, D. Qi, S. Yin, J. Bu, F. Li, C.F. Goh, S. Zhang, X. Chen, Adv. Mater. 25 (2013) 2957.
[5] Y. Meng, Y. Zhao, C. Hu, H. Cheng, Y. Hu, Z. Zhang, G. Shi, L. Qu, Adv. Mater. 25 (2013) 2326.
[6] S.K. Singh, M.K. Singh, P.P. Kulkarni, V.K. Sonkar, J.J. Grácio, D. Dash, ACS Nano 6 (2012) 2731.
[7] H. Wu, H. Shi, Y. Wang, X. Jia, C. Tang, J. Zhang, S. Yang, Carbon 69 (2014) 379.
[8] Y. Wang, Y. Shao, D.W. Matson, J. Li, Y. Lin, ACS Nano 4 (2010) 1790.
[9] M. Zhou, Y. Zhai, S. Dong, Anal. Chem. 81 (2009) 5603.
[10] S. Myung, A. Solanki, C. Kim, J. Park, K.S. Kim, K.B. Lee, Adv. Mater. 23 (2011) 2221.
[11] C. Peng, W. Hu, Y. Zhou, C. Fan, Q. Huang, Small 6 (2010) 1686.
[12] X. Sun, Z. Liu, K. Welsher, J.T. Robinson, A. Goodwin, S. Zaric, H. Dai, Nano Res. 1 (2008) 203.
[13] K. Liu, J.J. Zhang, F.F. Cheng, T.T. Zheng, C. Wang, J.J. Zhu, J. Mater. Chem. 21 (2011) 12034.
[14] K. Yang, S. Zhang, G. Zhang, X. Sun, S.T. Lee, Z. Liu, Nano Lett. 10 (2010) 3318.
[15] O. Akhavan, E. Ghaderi, S. Aghayee, Y. Fereydooni, A. Talebi, J. Mater. Chem. 22 (2012) 13773.
[16] K. Yang, J. Wan, S. Zhang, B. Tian, Y. Zhang, Z. Liu, Biomaterials 33 (2012) 2206.
[17] A. Sasidharan, L.S. Panchakarla, A.R. Sadanandan, A. Ashokan, P. Chandran, C.M. Girish, M. Koyakutty, Small 8 (2012) 1251.
[18] M. Fan, C. Zhu, Z.Q. Feng, J. Yang, L. Liu, D. Sun, Nanoscale 6 (2014) 4882.
[19] B.G. Kozen, S.J. Kircher, J. Henao, F.S. Godinez, A.S. Johnson, Acad. Emerg. Med. 15 (2008) 74.
[20] H.B. Alam, E. Koustova, P. Rhee, World J. Surg. 29 (2005) S7.
[21] N. Ahuja, T.A. Ostomel, P. Rhee, G.D. Stucky, R. Conran, Z. Chen, G.A. Al-Mubarak, G. Velmahos, M. deMoya, H.B. Alam, J. Trauma 61 (2006) 1312.
[22] C. Dai, Y. Yuan, C. Liu, J. Wei, H. Hong, X. Li, X. Pan, Biomaterials 30 (2009) 5364.
[23] C. Dai, C. Liu, J. Wei, H. Hong, Q. Zhao, Biomaterials 31 (2010) 7620.
[24] C. Fu, S. Wang, L. Feng, X. Liu, Y. Ji, L. Tao, S. Li, Y. Wei, Adv. Health Mater. 2 (2013) 302.
[25] R. Gu, W. Sun, H. Zhou, Z. Wu, Z. Meng, X. Zhu, Q. Tang, J. Dong, G. Dou, Biomaterials 31 (2010) 1270.
[26] S.B. Rao, C.P. Sharma, J. Biomed. Mater. Res. 34 (1997) 21.
[27] M.A. Worsley, P.J. Pauzauskie, T.Y. Olson, J. Biener, J.H. Satcher Jr., T.F. Baumann, J. Am. Chem. Soc. 132 (2010) 14067.
[28] J. Wang, M. Ellsworth, ECS Trans. 19 (2009) 241.
[29] X. Zhang, Z. Sui, B. Xu, S. Yue, Y. Luo, W. Zhan, B. Liu, J. Mater. Chem. 21 (2011) 6494.
[30] H. Sun, Z. Xu, C. Gao, Adv. Mater. 25 (2013) 2554.
[31] Y. Xu, Q. Wu, Y. Sun, H. Bai, G. Shi, ACS Nano 4 (2010) 7358.
[32] H. Hu, Z. Zhao, W. Wan, Y. Gogotsi, J. Qiu, Adv. Mater. 25 (2013) 2219.
[33] H. Bi, X. Xie, K. Yin, Y. Zhou, S. Wan, L. He, F. Xu, F. Banhart, L. Sun, R.S. Ruoff, Adv. Funct. Mater. 22 (2012) 4421.
[34] H.B. Alam, D. Burris, J.A. DaCorta, P. Rhee, Mil. Med. 170 (2005) 63.
[35] W.S. Hummers Jr., R.E. Offeman, J. Am. Chem. Soc. 80 (1958) 1339.
[36] J. Chen, K. Sheng, P. Luo, C. Li, G. Shi, Adv. Mater. 24 (2012) 4569.
[37] M.F. Shih, M.D. Shau, M.Y. Chang, S.K. Chiou, J.K. Chang, J.Y. Cherng, Int. J. Pharm. 327 (2006) 117.
[38] S.Y. Ong, J. Wu, S.M. Moochhala, M.H. Tan, J. Lu, Biomaterials 29 (2008) 4323.
[39] P.T. Sudheesh Kumar, V.K. Lakshmanan, T.V. Anilkumar, C. Ramya, P. Reshmi, A.G. Unnikrishnan, S.V. Nair, R. Jayakumar, ACS Appl. Mater. Inter. 4 (2012) 2618.
[40] L. Luo, G. Li, D. Luan, Q. Yuan, Y. Wei, X. Wang, ACS Appl. Mater. Inter. 6 (2014) 19371.
[41] K.H. Liao, Y.S. Lin, C.W. Macosko, C.L. Haynes, ACS Appl. Mater. Inter. 3 (2011) 2607.
[42] K.S.W. Sing, D.H. Everett, R.A.W. Haul, L. Moscou, R.A. Pierotti, J. Rouquerol, T. Siemieniewska, Pure Appl. Chem. 57 (1985) 603.
[43] M.D. Stoller, S. Park, Y. Zhu, J. An, R.S. Ruoff, Nano Lett. 8 (2008) 3498.
[44] P. Lian, X. Zhu, S. Liang, Z. Li, W. Yang, H. Wang, Electrochim. Acta 55 (2010) 3909.
[45] A. Shukla, J.C. Fang, S. Puranam, F.R. Jensen, P.T. Hammond, Adv. Mater. 24 (2012) 492.